JGP Journal of General Physiology

REVIEW

Combining elastic network models and linear response theory as tool to understand the global dynamics in allosteric regulation of HCN channels

Magnus Behringer[1], Jan Krumbach[1], Alessandro Porro[2], Andrea Saponaro[3], Dario DiFrancesco[2], Anna Moroni[2], Kay Hamacher[1,4], and Gerhard Thiel[1,2]

Hyperpolarization-activated cyclic nucleotide-gated cation channels (HCN channels) play important regulatory roles in the heart and the brain. At the core of their physiological functions is an activation by negative membrane potential and its modulation by cyclic nucleotides. While recent high-resolution cryo-EM structures combined with MD simulations have provided insights into fast events in the pore, like ion permeation, block, and cation-selectivity, the mechanism of slow allosteric regulation of gating by voltage and cyclic nucleotides remains poorly understood. Since slow conformational changes in proteins are largely determined by their global dynamics, coarse-grained computational methods such as elastic network models (ENMs) and linear response theory (LRT) analyses have been used to elucidate the intrinsic collective dynamics in HCN proteins associated with cyclic nucleotide-modulated gating. In this overview, we demonstrate the good performance of coarse-grained methods in predicting long-range conformational changes in HCN channels with respect to experimentally determined conformational states in these proteins with and without bound ligand. This provides general insights into the mechanical coupling of domains in HCN channels and on how their general tectonics enables bidirectional modulation between the binding site for cyclic nucleotides in the cytosol and the distant voltage-sensitive domain in the plasma membrane–embedded part of the protein.

Introduction

Hyperpolarization-activated cyclic nucleotide-gated cation (HCN) channels drive the "funny current," which controls pace-making in the heart (I_f) and repetitive firing in neurons (I_h) (Robinson and Siegelbaum, 2003; Saponaro and DiFrancesco, 2025). These mixed cation selective channels are present in humans in four isoforms (HCN1–4) and belong from a structural point of view to the superfamily of voltage-gated K^+ channels. Their monomers are typically made of a transmembrane part of the channel (TMPC) and a cytosolic part of the channel (CPC) (Fig. 1). The TMPC includes six transmembrane domains (TMDs S1–S4) in which TMD S1–S4 form the voltage sensor. In the tetrameric assembly of the functional channel TMDs S5 and S6 form the ion-conducting pore domain (PD) with the selectivity filter (SF) (Fig. 1). The CPC contains the so called HCN domain (HCND) at the N terminus and the cyclic nucleotide-binding domain at the C terminus, connected to the pore via a C-linker formed by "elbow" and "shoulder" (Fig. 1).

Despite their structural resemblance to outward rectifying Kv channels, HCN channels are inward rectifiers. The channel open probability increases with membrane hyperpolarization, providing conductance of a mixed K^+/Na^+ current, which is furthermore modulated by the concentration of cytosolic cyclic nucleotides (DiFrancesco and Tortora, 1991).

Binding of the second messenger cAMP to the CNBD increases the voltage-response of the channel and promotes opening at lower, more depolarized potentials. The physiological effect of a rise in the cytosolic concentration of the signaling molecules is an acceleration of pace making.

One challenge in understanding structure/function correlates in these physiologically important channels is how negative voltages can open a channel with the same basic architecture of outward rectifying Kv channels. A second related challenge is to unravel the allosteric nature of gating by both voltage in the voltage-sensing domains (VSDs) and ligand binding in the CNBD.

Major advances in understanding structure/function correlates in HCN channels were made by the acquisition of HCN structures with atomic resolution. While structures of the isolated CNBDs were already resolved some time ago (Zagotta et al., 2003; Xu et al., 2010; Lolicato et al., 2011; Akimoto et al., 2014; Puljung et al., 2014; Saponaro et al., 2014; Goldschen-Ohm et al.,

[1]Department of Biology, Technische Universität Darmstadt, Darmstadt, Germany; [2]Department of Biosciences, University of Milan, Milan, Italy; [3]Department of Pharmacological and Biomolecular Sciences, University of Milan, Milan, Italy; [4]Department of Physics, Technische Universität Darmstadt, Darmstadt, Germany.

Correspondence to Gerhard Thiel: thiel@bio.tu-darmstadt.de.

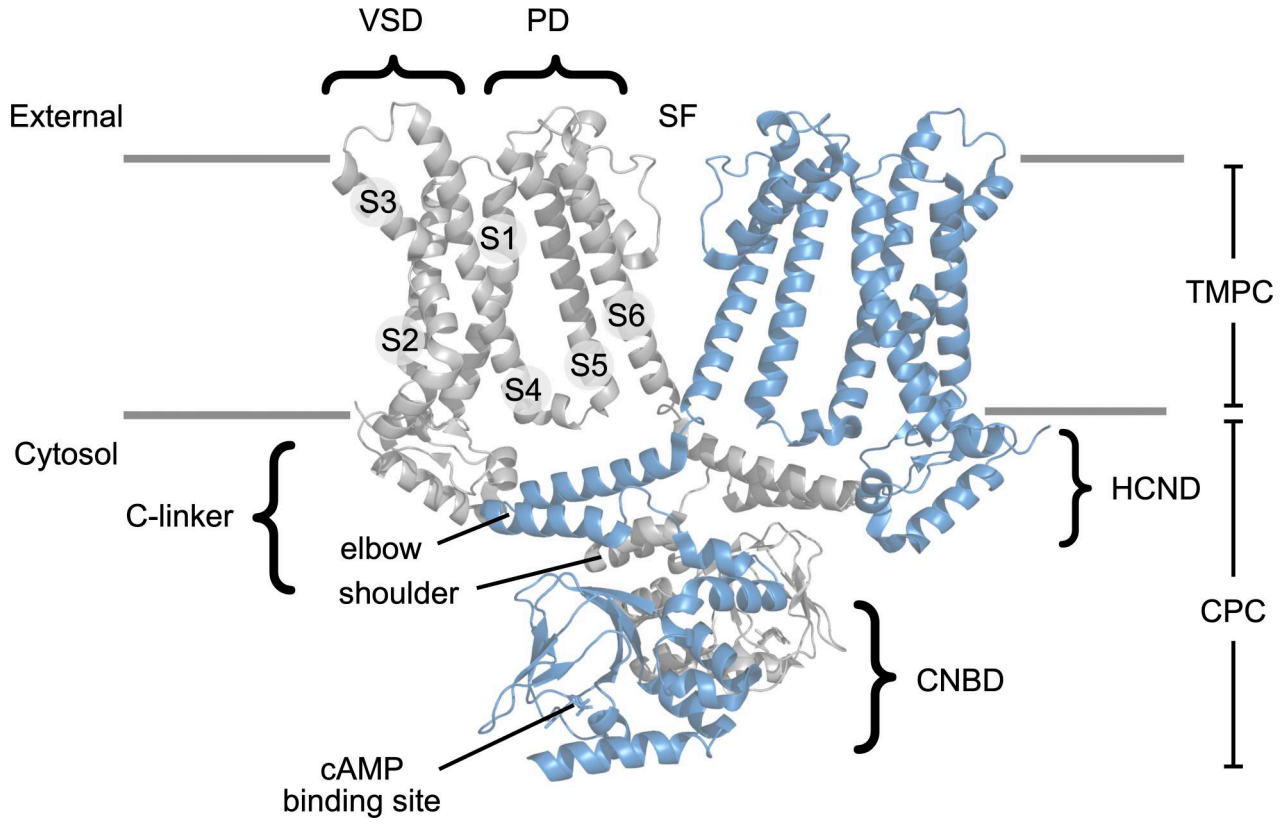

Figure 1. **General architecture and structural domains in HCN channels.** Side view of two opposite subunits of HCN4 channel in absence of cAMP (PDB accession no. 7NMN). Structural domains are indicated as follow: the TMPC includes voltage sensor (VSD), PD, and SF. The CPC includes: the N terminus HCND and at the C terminus, the C-linker formed by shoulder and elbow, that connects the cyclic nucleotide-binding domain (CNBD) to the PD. Transmembrane domains S1–S6 are indicated on the gray subunit; the position of the membranes is indicated by gray lines.

2016), recently also structures of HCN channels comprising the majority of the TMPC and the CPC became available. Currently, structures are known for HCN1 (Lee and MacKinnon, 2017; Lee and MacKinnon, 2019; Kim et al., 2024; Burtscher et al., 2024), HCN3 (Yu et al., 2024), and HCN4 (Saponaro et al., 2021), with and without cAMP in the ligand-binding site. Structures are available not only in the closed pore but also in the open pore state (Saponaro et al., 2021; Burtscher et al., 2024) as well as in states that resemble the voltage-activated state of the channel (Lee and MacKinnon, 2019; Burtscher et al., 2024). A list of the currently available HCN channel structures in the data bank is provided in Table 1.

Based on these high-resolution structural data, many functional features that are specific for HCN channels, like their low unitary conductance (DiFrancesco, 1986; Benndorf et al., 2025), their moderate K^+/Na^+ selectivity (Moroni et al., 2000; Lyashchenko and Tibbs, 2008), and their susceptibility to block by Cs^+ (DiFrancesco, 1982) and ivabradine (Bucchi et al., 2002), could be analyzed and understood at an atomistic level by MD simulations (Saponaro et al., 2021; Saponaro et al., 2024; Bauer et al., 2022; Krumbach et al., 2023; Benndorf et al., 2025).

While these simulations can cover dynamic events in a protein in time frames of nanosecond to maximal microsecond, they are not suitable to tackle the problem of slow structural transitions (Bahar et al., 2010). Such slow conformational changes with dwell times in the range hundreds of microseconds or even milliseconds, however, are dominating voltage and ligand-mediated gating in HCN channels. In addition to advanced time-resolved structural analysis of different conformational states in membrane transport proteins (Lee et al., 2025; Morgan et al., 2025), computational methods are also able to provide insights into such slow conformational changes in proteins (Shrivastava and Bahar, 2006; Hamacher and McCammon, 2006; Eom et al., 2007; Chennubhotla and Bahar, 2007; Bahar et al., 2010; Das et al., 2014; Hoffgaard et al., 2015; Zhao et al., 2024). Available data support the view that the conformational changes and allosteric mechanisms are intrinsically determined by the native fold of proteins, see e.g., Hamacher et al. (2006). The reason for this is that the geometry and topology of a protein under equilibrium conditions restrict its freedom of movement. Due to these inherent structural limitations, the fluctuations in proteins, which range from small local fluctuations to large collective movements of different domains or entire channel subunits in the gating process, are limited.

Here, we summarize recent attempts in understanding structure/function correlates of cAMP-mediated gating in HCN channels by means of such coarse-grained approaches. HCN channels are ideal systems for these kinds of studies because high-resolution structures are available for distinct functional states of the protein, like with and without cAMP bound. Also

Table 1. **List of PDB codes for currently available structures of HCN channel isoforms**

Isoform	PDB code	State	Mutations	Ligand/ Blocker/ Modulator	Modeled/ total residues	Resolution (Å)	Organism	Deposition author/s	Released
HCN1	5U6O	Voltage sensors in up configuration Closed pore	None	None	482/660	3.5	*H. sapiens*	Lee et al.	2017-01-25
HCN1	5U6P	Voltage sensors in up configuration Closed pore	None	cAMP	504/660	3.51	*H. sapiens*	Lee et al.	2017-01-25
HCN1	6UQF	Voltage sensors in down configuration Closed pore	F186C S264C	cAMP	531/660	3.04	*H. sapiens*	Lee et al.	2019-12-11
HCN1	6UQG	Voltage sensors in up configuration Closed pore	Y289D	cAMP	530/660	3.54	*H. sapiens*	Lee et al.	2019-12-11
HCN1	8T4M	Voltage sensors in up configuration Closed pore	F186C S264C	cAMP	533/890	3.16	*H. sapiens*	Burtscher et al.	2024-06-12
HCN1	8T4Y	Voltage sensors Intermediate configuration Closed pore	F186C S264C C309A	cAMP	501/890	3.58	*H. sapiens*	Burtscher et al.	2024-06-19
HCN1	8T50	Voltage sensors in down configuration Open pore conductive	F186C S264C	cAMP	474/890	3.6	*H. sapiens*	Burtscher et al.	2024-07-03
HCN1	8uc8	Voltage sensors in up configuration Closed pore	None	None	484/660	3	*H. sapiens*	Kim et al.	2024-07-31
HCN1	8uc7	Voltage sensors in up configuration Closed pore	None	Propofol	484/660	2.9	*H. sapiens*	Kim et al.	2024-07-31
HCN1	8Y60	Voltage sensors in up configuration Closed pore	None	Ivabradine Cholesterol	473/890	3.23	*H. sapiens*	Che et al.	2025-10-29
HCN1	9BC6	Voltage sensors in up configuration Closed pore	M305L	Propofol	484/660	2.5	*H. sapiens*	Kim et al.	2024-07-31
HCN1	9BC7	Voltage sensors in up configuration Closed pore	M305L	cAMP	506/660	3.3	*H. sapiens*	Kim et al.	2024-07-31
HCN3	8INZ	Voltage sensors in up configuration Closed pore	None	VX9[a]	465/774	2.72	*H. sapiens*	Yu et al.	2024-04-10
HCN3	8IO0	Voltage sensors in up configuration Closed pore	None	cAMP	473/774	3.19	*H. sapiens*	Yu et al.	2024-11-13
HCN4	6GYN	Voltage sensors in up configuration Closed pore	None	None	495/521	3.4	*H. sapiens*	Shintre et al.	2019-05-08
HCN4	6GYO	Voltage sensors in up configuration Closed pore	None	cAMP	501/521	3.4	*H. sapiens*	Shintre et al.	2019-05-01
HCN4	7NMN	Voltage sensors disconnected from the pore Open pore	None	None	469/889	3.6	*Oryctolagus cuniculus*	Chaves-Sanjuan, A.	2021-06-30

Table 1. **List of PDB codes for currently available structures of HCN channel isoforms (*Continued*)**

Isoform	PDB code	State	Mutations	Ligand/ Blocker/ Modulator	Modeled/ total residues	Resolution (Å)	Organism	Deposition author/s	Released
HCN4	7NP3	Voltage sensors in up configuration Open pore conductive	None	None	490/892	3.3	*O. cuniculus*	Giese et al.	2021-08-11
HCN4	7NP4	Voltage sensors in up configuration Closed pore	None	cAMP	501/892	3.3	*O. cuniculus*	Giese et al.	2021-08-11
HCN4	8OFI	Voltage sensors in up configuration Open pore conductive	None	Ivabradine	452/892	3.6	*O. cuniculus*	Saponaro et al.	2024-08-14

All structures were obtained by single particle cryo-EM and comprise most of the channel proteins (see Modelled/total residues) with transmembrane (TMPC) and cytosolic part (CPC); in all cases, the flexible C and N termini remained unresolved. Structures were obtained without (apo) and with (holo) the natural ligand cAMP bound; in presence of the open-pore blocker (ivabradine) or potential modulators (propofol, cholesterol, and VX9). All proteins were isolated from non-polarized membranes (0 mV) and likewise solved without imposing voltage. In some cases (6UQF/6UQG; 8T50), prior to isolation, the S4 domain was fixed by metal cross-bridging in a down configuration mimicking the hyperpolarized-activated position. In most cases, the pore is in the closed state; for three cases (8T50; 7NP4; 8OFI), the pore is open and conductive (MD simulations).
[a]VX9:4-[[(2S,4aR,6S,8aS)-6-[(4S,5R)-4-[(2S)-butan-2-yl]-5,9-dimethyl-decyl]-4a-methyl-2,3,4,5,6,7,8,8a-octahydro-1H-naphthalen-2-yl]oxy]-4-oxidanylidene-butanoic acid.

structures with the voltage sensor in the nonactivated and activated conformation are available (Table 1). In this sense, the starting and end points of conformational transitions in HCN channel gating are well-defined by experimental data, and coarse-grained computational approaches can provide insights into the mechanisms and into the mechanics for the transition between these states. We show here that elastic network models (ENMs) like Gaussian network models (GNMs) and similar models (Haliloglu et al., 1997; Tirion, 1996), and in particular their extension to anisotropic network models (ANMs) (Atilgan et al., 2001), were, in combination with linear response theory (LRT) (Ikeguchi et al., 2005), able to reveal the mechanic coupling between domains in these proteins. This analysis provides insight into the dynamics of allosteric changes in these channels upon cAMP binding.

Description of computational methods

The analysis of ENMs is based on the finding that large dynamic motions in a protein are determined by geometric constrains inherent in the three-dimensional architecture of a polypeptide. These motions, which are dictated simply by the global fold of a protein, are presumably the basis for functional properties such as ligand binding or sensing of physical cues like pressure or voltage. A coarse-grained representation of the contact topology in a protein of interest in an ENM (Bahar et al., 2010) should, together with LRT (Ikeguchi et al., 2005), provide the information of such global motions in relation to function. In combination with their low computational costs both methods are ideal for understanding the mechanical interactions and long-range conformational changes in complex proteins. With these features both approaches are particularly interesting for understanding interactions in HCN channels between the cytosolic CNBD and the distant membrane-resident VSD (Fig. 1).

ENMs analysis

The native state of a protein is described by the ensemble of its conformational states. These are constantly fluctuating around an equilibrium and all together sample the native fold of a protein (Atilgan et al., 2001; Hamacher and McCammon, 2006; Lezon et al., 2009; Bahar et al., 2010; Mahajan and Sanejouand, 2015). These fluctuations are not only accounting for the passive motions in a protein but also for functionally relevant movement of domains such as those involved in ligand-binding, allosteric regulation, and cooperativity (Lezon et al., 2009; Bahar et al., 2010). In the specific case of HCN channels this could, for example, be complex movements such as voltage-dependent gating, which requires highly collective global motions of the voltage sensor relative to the pore. Such global conformational changes of a protein strongly correlate to its normal modes (Lezon et al., 2009; Bahar et al., 2010). A protein has many modes of which each one represents a different pattern of atomic displacements characterized by a distinct frequency with which it oscillates back and forth (Mahajan and Sanejouand, 2015). Most relevant for the protein's mechanical functionality are the modes with the lowest frequencies. They are the most interesting for the investigation of protein dynamics since these slow vibrations also generate the largest amplitudes (Atilgan et al., 2001; Hayward and de Groot, 2008; Bahar et al., 2010; Kondrashov, 2011; Sanejouand, 2013). It has been shown that they are responsible for 90–95% of atomic displacements in proteins (Sanejouand, 2013). The relevant normal modes, which are dominating global changes in a protein, can be examined with an ENM (Atilgan et al., 2001; Bahar et al., 2010). The starting point of every ENM is the native fold of a protein obtained from X-ray crystallography, cryo-EM, or NMR. The high-resolution structures with all atomistic coordinates, which are currently available for HCN channels in different functional states, are listed in Table 1. These structures can be

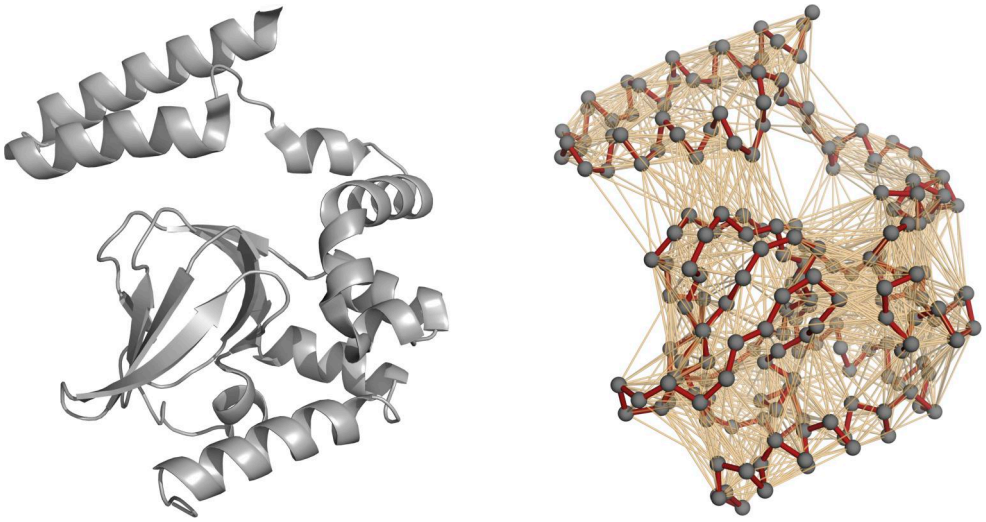

Figure 2. **Illustration of an ENM of the C-terminal domain of the HCN4 channel.** Crystal structure of CNBD from HCN4 (PDB accession no. 3U11) (left). In the network model (right), each amino acid from the structure is represented by a bead centered at its C_α atom. The covalent bonds (red lines) and all nodes within a specified cutoff distance of each other (here: 13 Å) are connected by springs (orange lines).

used to build coarse-grained models in which each residue is represented by a single node, usually coincident with the C_α atom. All nodes are connected by a spring, if their distance is smaller than a cutoff distance (Hayward and de Groot, 2008; Kondrashov, 2011; Sanejouand, 2013). Therefore, the model does not distinguish between covalent and non-covalent interactions but purely on distance between two nodes.

Fig. 2 shows an example for the transformation of the crystal structure of the CNBD from HCN4 (PDB accession no. 3U11) into an ENM. Each amino acid in the polypeptide is represented by a bead (=node) centered on its C_α atom. All nodes are connected by springs when their distance is smaller than 13 Å, in this case. Backbone connections are displayed in red just for visualization purposes.

To model the interaction between two nodes, e.g., to describe its spring-like character, Newton's equations of motion have to be solved. Since this is analytically impossible, they need to be approximated, which can be done with a Taylor expansion if the displacements in the vicinity of the equilibrium are small enough. The constant term can be neglected as only differences in the potential energy and not absolute values are of interest. The linear term vanishes too since local minima require the first derivative to be zero. By construction the equilibrium/native state is such a minimum. That leaves the quadratic term as higher derivatives result in even smaller contributions to the potential energy and are thus ignored, too (Sanejouand, 2013). This implies that an ENM is the most general model of biomolecular mechanics—given that the interaction strengths (spring constants) are well chosen.

Generally, there are two classical approaches for using ENMs, which are either GNM or ANMs (Atilgan et al., 2001; Bahar et al., 2010; Sanejouand, 2013). The latter additionally allows to compute the direction of movement.

An ANM's total potential energy V is given by

$$V = \frac{\gamma}{2}\sum_{|r_{ij}^0|<R_c}\left(r_{ij}-r_{ij}^0\right)^2 \quad (1)$$

the sum of the squared fluctuations with r_{ij} being the actual distance between nodes i and j and r_{ij}^0 being their distance in the experimental structure while only considering r_{ij}^0 if smaller than the cutoff distance R_c (Hayward and de Groot, 2008; Kondrashov, 2011; Sanejouand, 2013). In the case of biomolecules, a cutoff distance of 13 Å is frequently used, as it was found empirically to give the best fit of the coarse-grained models to all-atom MD simulations (Atilgan et al., 2001). The force constant γ is usually chosen to be the same for all interacting pairs. In the classical ANM, this uniform value is neither distinguishing between different types of amino acids nor between the nature of their interactions because collective motions are dominated by the topology of the native structure.

The interaction potential (1) is the modeling part. In a second step, one has to understand the dynamics induced by it. Typically, this is done by extensive MD simulations. ENMs are, however, explicitly constructed to avoid the need for such time-intensive simulations. Instead, we develop the potential in a Taylor series of polynomials of all coordinates of the amino acids. The first and constant term is uninformative as the physical effects manifest themselves in energy differences, where the first term would cancel itself. The first-order term vanishes by construction as the input structure is assumed to be in the minimal energy state and in a compact domain the first derivative vanishes at extremal points. This leads us to the second-order term that mimics harmonic, spring-like interactions.

To extract information from conformational changes in an ANM, the second derivatives of the potential energy are then calculated for each pair of nodes i and j that are connected with respect to their three dimensions. This leads to the 3 × 3 submatrix H_{ij} with

$$H_{ij} = \begin{pmatrix} \frac{\partial^2 V}{\partial x_i \partial x_j} & \cdots & \frac{\partial^2 V}{\partial x_i \partial z_j} \\ \vdots & \ddots & \vdots \\ \frac{\partial^2 V}{\partial z_i \partial xj} & \cdots & \frac{\partial^2 V}{\partial z_i \partial z_j} \end{pmatrix} \quad (2)$$

This is calculated for all interacting atoms/nodes resulting in an NxN matrix consisting of 3 × 3 sub-matrices. Taken together, this results in a 3N × 3N shaped matrix called the Hessian. From this, the singular values and vectors can be computed using a singular value decomposition algorithm (Press et al., 2007). In total, the protein has 3N singular values with the first six values vanishing as they correspond to the three translational and three rotational degrees of freedom (Wilson, 1941). These six values are not of interest since the goal of the analysis is to investigate the conformational fluctuations within the molecule rather than translation and rotation of the whole molecule. Of the remaining 3N-6 singular values, typically the first values, namely the lowest ones, correspond to low-frequency motions. They represent the global structural changes with higher amplitudes, which were shown to be the functionally relevant ones (Hayward and de Groot, 2008; Sanejouand, 2013).

An extension of the ANM, the extended ANM can be employed (Hamacher and McCammon, 2006). Instead of a uniform force constant γ, a distinct term for each contact potential has been included in this network model, which pays respect to the type of amino acid but also to the type of interaction between two nodes. The latter is described by two features, the bond type (covalent vs. non-covalent) and the relative location of interacting nodes (interchain vs. intra-chain). In this way it is possible to weight, for example, covalent interchain interactions or disulfide bonds differently from weak intra-chain interactions. They also distinguish between the difference in hydrophobic force that is experienced by intra-chain interactions versus inter-chain interactions (Hamacher and McCammon, 2006).

LRT

The LRT assumes that an external perturbation of a protein will evoke a linear response in its structure. This means that the protein will undergo a conformational change proportional to the strength of the perturbation. Examples for perturbations in an HCN channel are (1) the impact of an electrical field on the voltage sensor domain or (2) the binding of a ligand to a specific binding site. Therefore, it should be possible to predict the conformational transition in HCN channels between the apo- and a holo-form from the analysis of the normal modes. This information will again be contained in the Hessian of an appropriate ANM.

The change in the positions Δr_i for amino acid i reads

$$\Delta r_i \cong \beta \sum_j \langle \Delta r_i \Delta r_j \rangle_0 f_j \quad (3)$$

where β is $1/k_B T$ with the Boltzmann constant k_B and the absolute temperature T. $(\Delta r_i \Delta r_j)_0$ is the covariance matrix in the unperturbed state, and f_j is the force acting on amino acid j. See Ikeguchi et al. (2005) for a detailed derivation.

This equation can now be simplified since at constant temperature and within the harmonic approximation of ANMs near the equilibrium the covariance matrix is proportional to the Hessian matrix H (Penrose, 1955; Ikeguchi et al., 2005; Hayward and de Groot, 2008). Thus, the spatial shift of the positions of all amino acids $\Delta\vec{p}$ as an 3N-dimensional vector is

$$\Delta\vec{p} = H^{-1}\vec{F} \quad (4)$$

where H^{-1} is the inverse Hessian matrix, and the external force of the perturbation is the 3N-dimensional vector $\vec{F}$ acting on the protein (Ikeguchi et al., 2005; Kunzmann et al., 2024).

A simple prediction from this model is that binding of a ligand exerts distinct forces on the target protein by interacting with critical residues in the binding site (Fig. 3). Hence, in a computational approach, it should be possible to mimic in HCN channels the impact of cAMP binding to the CNBD on the remaining protein by application of forces to these critical sites in an ENM (Fig. 3). For several proteins, it was already confirmed that these predicted displacements by LRT were, despite the simplicity of this approach, in very good agreement with experimental X-ray and cryo-EM data as well as all-atom MD simulations (Hamacher et al., 2006; Hamacher, 2011; Groß et al., 2017; Groß et al., 2018). For the present review, it is worth mentioning that the accuracy of conformational changes by LRT is even valid for membrane proteins where the membrane was neglected (Das et al., 2014).

In classical LRT, forces are applied to residues in a protein with the intention of mimicking known perturbations to the protein. To contextualize the displacements given by an LRT in an unbiased way, a "null model" of perturbation had been developed (Groß et al., 2017; Groß et al., 2018). Its purpose is to test if the chosen force vector with the directionality of interest is the only one producing particular conformational changes. In this procedure, forces are applied to the residue or residues of interest in all possible directions (Fig. 3). In the case of HCN channels, this could, for example, be the cAMP-binding site. The consequence of these forces on the conformation of the target protein like the conformation of a ligand-binding site are then recorded and clustered according to their directions. Whenever the shifts caused by forces with a different direction than the one of interest cause shifts other than those expected, the LRT result is relevant to the mechanics of the molecule.

Finally, the predicted conformations are compared with experimentally known conformational changes in the protein. Fig. 3 i shows the movement following ligand binding to a hypothetical protein like the CNBD in HCN channels. Fig. 3 ii shows the LRT simulation of ligand binding, producing the same movement. In the null LRT model, shown in Fig. 3 iii, the application of a distinct force, which is represented by the red vector, shifts the ligand-binding domain from an open into a closed conformation, while other forces, represented by green, blue, and light blue vectors, do not. This shows, in turn, that the process of ligand binding will generate a conformational change in the direction of the red vector. In this case, it is possible to evaluate the flow of conformational information over long distances in a protein; in HCN channels, this could be the flow of information between CNBD and VSD. Such a null model

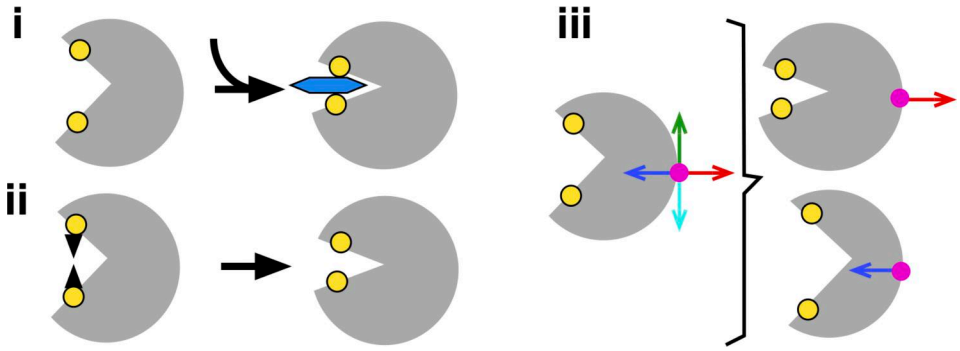

Figure 3. **Principle of LRT. (i)** Sketch of experimental structure of a protein in ligand-free (left) and -bound (right) conformation in which ligand (blue) interacts with two critical residues (yellow). **(ii)** LRT simulation of ligand binding. Forces (black arrows) are applied to critical residues to obtain holo-form of binding site. The predicted conformation of the binding site from the simulation should mimic the experimental holo structure. **(iii)** In the null LRT model forces are applied in all possible directions to a critical residue (purple) distant from the ligand-free binding site. The conformational change from different force directions are then compared with experimental structures. In that case, the red vector shifts the conformation of the binding site toward its holo-form, while the blue vector initiates a shift in the opposite direction. Hence, ligand binding will presumably exert a force on the critical residue in the direction of the red vector.

approach was first developed for a monomeric protein (Groß et al., 2017). So, to study the conformational changes in case of a tetrameric channel like HCN, it has to be applied to each subunit simultaneously or to individual monomers when examining potential cooperativity (Groß et al., 2018; Kunzmann et al., 2024).

Reduced models cannot cover the full dynamics

It is important to note that reduced molecular models such as ENMs cannot reproduce the full dynamics of a protein in detail. For example, the assumption of purely harmonic interactions ("springs") prevents the application of ENMs to large conformational changes, (Miyashita et al., 2003) like, in particular, the "breaking" of contacts. Such a breaking arises, e.g., in large conformational changes so that residues move further apart than the threshold distance upon which in the model no interaction is possible anymore.

First of all, such larger movements might bring the structure into a state where the Taylor expansion to second order (harmonic interactions) is insufficient. Incorporating additional terms, on the other hand, hinders the efficient solution via the singular value decomposition. The respective equations of motions would need to be solved just as traditional MD programs do.

Secondly, breaking of contacts cannot be investigated, as this changes the Kirchhoff and the Hessian matrix, respectively. While some work has be done to merge two or more distinct ENMs—capturing the dynamics of some open or closed state, for example—the overall insight into the transition state remains illusive (Miyashita et al., 2003).

The same applies to the application of LRT: scenarios in which ENM and LRT can give insight into the dynamics of proteins are restricted to movements around the native fold. However, this could still provide clues to the precursors of larger conformational changes.

Mechanical transmission between CNBD and transmembrane domains in HCN channels

The challenge of understanding allosteric gating in HCN channels is that the VSDs as well as the gates, which determine the voltage-sensitive opening of the channel, are in the TMPC. The ligand-binding domains on the other hand, which modulate the voltage-dependent channel opening, are in the cytosolic domain, e.g., in molecular terms far away from the VSD and the gates (Fig. 1). The key question is how conformational changes in the ligand-binding domain are transmitted to VSD and/or channel gates for a modulation of voltage dependency.

Even before high-resolution structures of HCN channels, including both TMPC and CPC, were available, there was already a bulk of structural information on their isolated CNBDs in holo and apo state (Zagotta et al., 2003; Lolicato et al., 2011; Saponaro et al., 2014). These studies had uncovered the cAMP-binding site as well as the amino acid side chains, which mediate ligand binding in the CNBDs of different HCN channels. Analysis of the cAMP-bound versus -unbound structures had furthermore identified complex rigid body movements of helical domains in the CNBD together with a stabilization of several of the helices in response to binding and unbinding of cAMP (Saponaro et al., 2014). To obtain information on how such ligand-induced local conformational changes in the CNBD are mechanically transmitted to the channel domain in the membrane, Weißgraeber and co-workers (Weißgraeber et al., 2017) performed a coarse-grained molecular analysis on a homology model, comprising the CNBD of HCN4 and the channel domain of the Kv1.2 channel. This was motivated by the idea that such a homology model was sufficiently accurate to provide, in the absence of structural details on the HCN transmembrane part, information on basic mechanical connections between the ligand binding and the channel domain. To this end, an ENM was constructed from the Kv1.2/HCN4 chimera, and the LRT approach (Ikeguchi et al., 2005) was used to mimic the local conformational changes in the CNBD, which are elicited by unbinding of cAMP from its binding site. For this purpose, an external force was applied in

each of the four monomers to the six residues in the binding site, which interact with cAMP. This force was tailored such that it caused a distortion of the cAMP-binding site, which mimics the experimentally determined conformation of the unbound state (Saponaro et al., 2014).

Comparative analysis of the ENM with and without this external force revealed interesting short- and long-range movements in the channel protein in response to the local conformational changes in the cAMP-binding site. These conformational changes were not confined to the CNBD but also transmitted via strong rotational movements into the TMPC; notably, only the SF occurred structurally, unaffected by the release of cAMP from its binding site (Weißgraeber et al., 2017).

The data also highlight interesting bidirectional interactions between the C-linker of the CNBD with the cytosolic short linker that connects the transmembrane domains S4 and S5. The most striking observations were torsion like movement of the C-linker away from the TMPC in response to release of cAMP from the binding site (Fig. 4 and Video 1). With the C-linker as a mechanical transmitter between the CNBD and TMPC, a torsion-like movement of the cytosolic domain is than translated into a twist-like motion at the inner gate of the channel (Weißgraeber et al., 2017). Because such an iris-like motion has already been causally linked to the gating in other K^+ channels (Marchesi et al., 2018), the computational data predict that the same kind of mechanical connection between cAMP-binding site and channel is also part of the allosteric mechanism in HCN channels which couples cAMP- and voltage-dependent gating.

These predictions were made based on a crude homology model and may therefore not hold true for the real structure of an HCN channel. But when the first high-resolution cryo-EM structures of HCN1 in the apo- and holo-conformation (Lee and MacKinnon, 2017) were published, it turned out that the predictions from the ENM/LRT analysis perfectly met the structural findings. The model predicted iris-like movement of the C-linker (Fig. 4 and Video 1) was indeed confirmed by an inspection of the structures of this domain in the presence and absence of cAMP (Fig. 5 C) (Lee and MacKinnon, 2017; James and Zagotta, 2018). The linker of the holo- and the apo-structure exhibit the same rightward iris-like rotation that was predicted from the LRT analysis (Weißgraeber et al., 2017). This good agreement between experimental and computational data underscores the high information content of the coarse-grained approach. It also shows that mechanical connections, which are important for channel gating in HCN channels, are presumably inherent features of the global structure of these proteins and independent of structural details.

The recent availability of high-resolution structures of HCN1 channel with TMPC and CPC (Table 1) paved the way for a more detailed and more realistic analysis of their structure/function correlates. To tackle the mechanism of allosteric gating, Groß and co-workers (Groß et al., 2018) applied the perturbing force in the ENM of the HCN1 channel, the perturbating force of LRT method, not in the cAMP-binding site but further upstream in a single position on the so-called elbow (Zagotta et al., 2003; James and Zagotta, 2018), a critical site in the bend between the A′ and B′ helices of the C-linker. It is well established that the C-linkers are packed in a channel tetramer in an elbow on the shoulder configuration in which the A′ and B′ helix from one subunit interact with the C′ and D′ helix of the adjacent subunit. Hence, the elbow is a key strategic position for imposing a conformational change in the C-linker, e.g., the mechanical element, which connects the CNBD to the TMPC (Zagotta et al., 2003; James and Zagotta, 2018). With this architecture, a realistic perturbation of the elbow by LRT should mimic binding/release of cAMP to/from the binding site; in the domain that connects the CNBD with the membrane-embedded part of the protein, this system should report the respective conformational changes transmitted to the TMPC. A comparison of the structural transition between HCN1 apo- and holo-structure with a computational perturbation of the elbow horizontally and away from the central axis shows the same rotational motion of the CNBD (Fig. 5). This again highlights the very good agreement of computational and experimental data. As a further quality confirmation of the approach, it was also observed that the local application of a force on the elbow, which mimics the transition from the holo-to-the-apo-configuration, also affects the conformation of the cAMP-binding site. As expected for a reciprocal system, the distortion in the downstream direction of the elbow causes an "apo like" conformation of the cAMP-binding site.

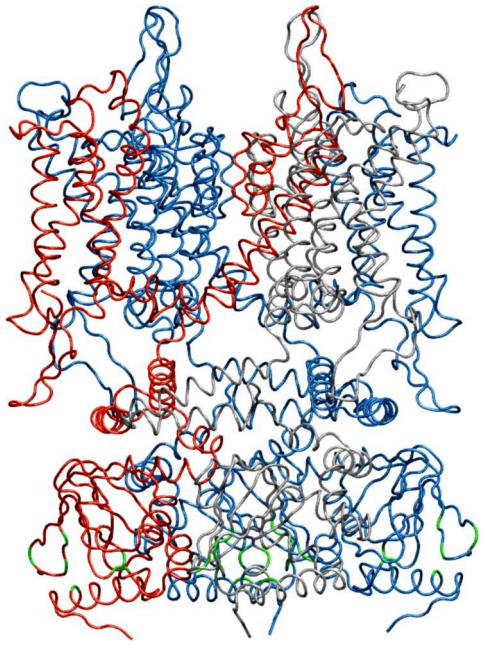

Figure 4. **Concerted movements in a synthetic HCN channel chimera following release of cAMP from its binding site.** Morphing video on concerted movement of CNBD and C-linker relative to transmembrane domains of a synthetic HCN channel. Morphing was obtained from computational data using LRT analysis of the Kv1.2/HCN4 chimera after force application to all four cAMP-binding pockets to mimic the release of cAMP from its binding site (Weißgräber et al., 2017). For visualization of the movements of CNBD and C-linker relative to the transmembrane domains, the latter have been fixed. The side view perspective predicts that the holo-to-apo-transition elicits a rotational movement of the CNBD and the C-linker relative to the transmembrane domains. In this context, the latter undergoes a pronounced iris-like rotation around a central axis.

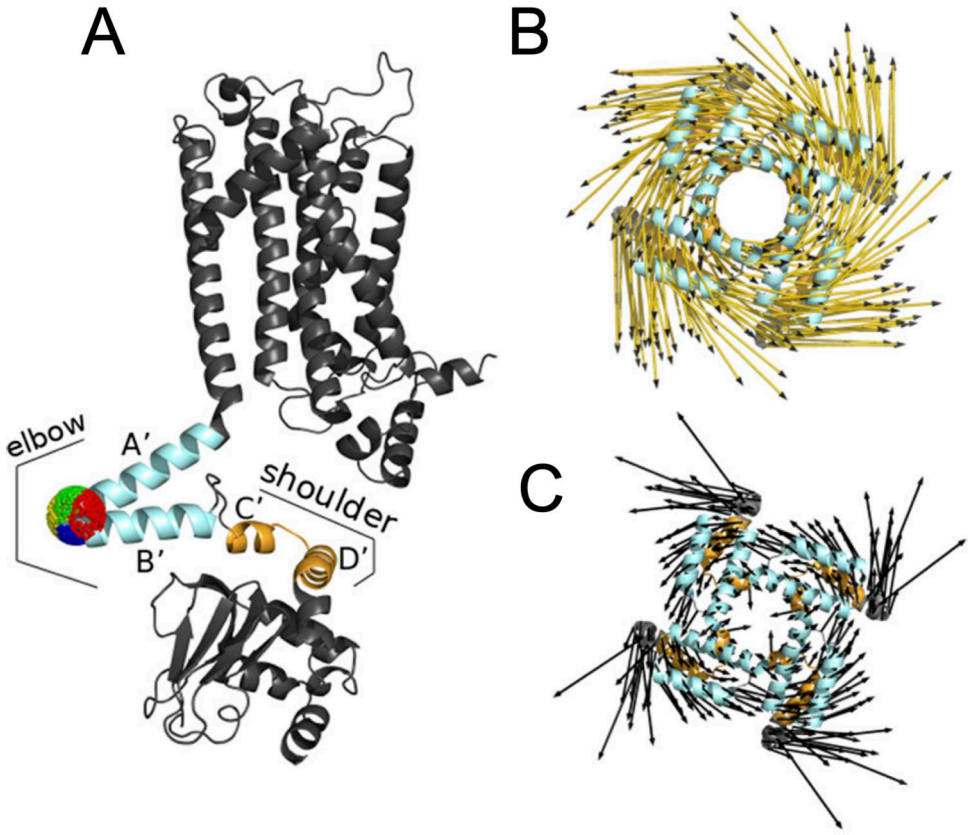

Figure 5. **Comparison of predicted and experimentally measured displacements of the C-linker in cAMP-free and cAMP-bound HCN1 channel. (A)** Perturbation forces in different directions applied to Ala-425 at the tip of the so-called elbow in the C-linker. Perturbation directions were sorted in four different clusters (red, blue, yellow, and green) depending on their conformational impact on the "shoulder domain." **(B)** Predicted displacements of C-linker from LRT analysis following perturbation at Ala-425 force in direction of yellow arrows in A. **(C)** The predicted displacement vectors in B mimic the experimentally observed iris-like leftward movement in the apo-to-holo-transition of HCN1 cryo-EM structures. The arrows indicate the direction of the respective displacement, while their overall magnitude (length) is uninformative (arbitrary units); however, the ratio of their lengths is a quantifier. Visualizations are top views from an extracellular perspective. Data, with permission, are reproduced by Groß et al. (2018).

These findings confirm that the tip of the elbow is indeed a critical position for the mechanical transduction of information from the CNBD to the pore and vice versa. This good agreement between computational data and experimental structures as well as the reciprocal nature of conformational changes in the CNBD/C-linker domain are a strong indication that also the conformational changes in the TMPC are relevant for understanding the impact of the CNBD on voltage-dependent gating.

A close view on the computational data advocates the following model: The membrane embedded TMPC is constrained in its movement particular in the z direction by the lipid bilayer. CNBD and C-linker on the other hand are free to move in all directions. In the transition between apo- and holo-state the CNBD undergoes an anticlockwise rotation with respect to the PD, bringing the CNBD closer to the membrane. This presumably favors direct contacts between the CNBD and residues in the TMPC, including the S4 domain in the VSD (Weißgraeber et al., 2017). Because of the different degrees of freedom the iris-like motion of the CNBD is also transmitted further to the inner gate, which is in direct contact to the C-linker. This process is presumably guided by simple mechanical forces.

Important to mention here is that these predicted complex conformational changes, including the iris-like motion of the CNBD and the change in the distance between the latter domain and TMPC were independently confirmed by high-speed atomic force microscopy studies on the related cAMP gated SthK channel (Marchesi et al., 2018). The latter study reports the same kind of a ligand-triggered iris diaphragm mechanism of C-linker motion that is predicted by the ENM/LRT analysis of HCN structures (Weißgraeber et al., 2017; Groß et al., 2017). We can take this as additional evidence for the basic assumption of this review namely that the three-dimensional geometry and topology in the protein under equilibrium conditions determines the direction and degree of freedom in movements.

It is well established that cAMP binding is insufficient to open HCN channels in the absence of movement of the VSD by negative voltage (Flynn and Zagotta, 2018). Hence, the impact of the iris-like motion of the CNBD following ligand binding on the TMPC bears no direct information on the primary mechanism of HCN channel opening. Nonetheless, we can expect that the induced conformational changes in the TMPC contains information on how ligand binding facilitates voltage-dependent channel opening.

One important information from the LRT data was that all transmembrane domains do not undergo vertical movements but

rather distinct tilting motions. This finding predicted a scenario, which was later confirmed by experiments (Lee and MacKinnon, 2019), namely that the S4 domain is not undergoing a rigid-vertical movement in the direction of the electrical field but a tilting motion coupled with a downward movement of the S4 helix, approximately two helical turns relative to the charge transfer center. The same movements, though less pronounced, were later confirmed in experimental structures (Burtscher et al., 2024). Tilting of S4 and the concerted movements of S5 in the opposite direction suggest a scenario in which the ligand-binding status in the CNBD can favor the formation or collapse of a water-filled internal "gating" canal by long distance interactions. Previous work had highlighted the importance of this gating canal between S4 and S5 for voltage-dependent opening of HCN channels (Bell et al., 2004). It was postulated that the shape of this aqueous gating canal would affect the membrane field surrounding the S4 segment and influence in this manner the voltage dependency of the channel (Bell et al., 2004). Hence, the CNBD could have in this way an indirect impact on voltage gating; ligand binding could favor widening of the aqueous gating canal and, in this manner, lower the energy for voltage-dependent channel opening.

A further positive impact of ligand binding on HCN channel opening can be deduced from the effect of the iris type motion of the CNBD at the exit from the channel's cavity. From structural and experimental data, it had been speculated that HCN channels have an inner gate at the entry from the cytosol into the cavity (Rothberg et al., 2003). This gate was thought to be narrow at depolarized voltages and widened upon hyperpolarization, allowing the passage of ions. A recent cryo-EM structure has confirmed this picture, showing that a small widening of this constriction at the entry of the HCN4 channel is sufficient for transforming the closed channel into a conductive open channel (Saponaro et al., 2021). In MD simulations, this protein exhibits all major functional properties of the HCN4 channel known from experimental studies (Saponaro et al., 2021; Saponaro et al., 2024; Bauer et al., 2022). After determining that cAMP binding and its lateral pushing force on the C-linker elbow also affect conformations in the TMPC, Groß and co-workers (Groß et al., 2018) examined the consequent changes on the radius of the inner gate. This showed that the mechanical motions of the CNBD following ligand binding were indeed favoring a widening of this part of the inner gate. Perturbations in all other directions caused a narrowing of the inner gate. Since cAMP binding by itself is not sufficient to open HCN channels, these data must be interpreted again in the context of a stabilizing effect of cAMP on the open state of the channel. A similar interpretation for the role of cAMP in HCN gating was already proposed based on experimental data (Craven and Zagotta, 2004; Craven et al., 2008; James and Zagotta, 2018).

The HCND acts as a sliding crank and transmits horizontal movement of the C-linker into tilting movements of transmembrane domains

The first HCN1 structure obtained by cryo-EM (Lee and Mackinnon, 2017), highlighted the presence of a folded domain comprising three helices (α, β, and γ) in their cytosolic N terminus (Fig. 1). The structural organization of this domain, now known as HCND, suggested that it serves for a mechanical coupling between the C-linker and the VSD in these channels. Functional data on voltage- and cAMP-dependent gating, in combination with mutations, proposed that the HCND presumably serves as a sliding crank that transmits the movement between the C-linker and the VSD, once the C-linker is rotating in response to cAMP binding to the CNBD. The β helix of the HCND is on one end connected via salt bridges to the B′ and A′ helices of the C-linker. On the other end, the β helix forms a hydrophobic interaction with the lower end of the S4 domain via a phenylalanine residue on HCND that is inserted in a hydrophobic pocket between S1 and S4. With these connections, the HCND converts the planar iris-like rotational movement of the C-linker into a tilting displacement of the VSD (Porro et al., 2019).

The combination of ENMs and LRTs served as a perfect tool for testing these predictions. For this purpose, the same force, which mimics the aforementioned conformational changes induced by cAMP binding (Groß et al., 2018), was applied to the channel protein. This resulted in a concerted displacement of the C-linker together with the HCND with the effect that both domains rotate with a similar angle to the z-axis. This rotational movement of the C-linker and the HCND was then transmitted to the VSD, where it causes a distinct tilting of the S4 (Porro et al., 2019). The coupled motions of C-linker, HCND and S4 derived from the LRT analysis are illustrated in Fig. 6, A and B.

In the context of HCN gating, the prediction that cAMP binding favors tilting of the S4 domain is most interesting. Notably, tilting with a kink formation of the S4 domain was also proposed in experimental and computational studies as a crucial step in the voltage-dependent activation of HCN channels (Kasimova et al., 2019; Lee and MacKinnon, 2019; Elbahnsi et al., 2023). Fig. 6 C, i–iv, show the S4 domain from cryo-EM structures of HCN1 in the depolarized close and in a presumed hyperpolarized-like pre-open state, obtained by forcing the voltage sensor in the downward conformation with covalent bonds (Lee and Mackinnon, 2019). Within major global structural changes between the two conformations, it occurs that the S4 domain is nearly linear in the depolarized state but kinked in the hyperpolarized state; amino acid Ser272 serves as hinge for a bending of the lower part of the helix away from the pore axis. Fig. 6 C, iii and iv, illustrate the predicted conformations of the same domain from an LRT analysis of HCN1 before and after application of a force on the CNBD, which mimics the effect of cAMP binding (Groß et al., 2018; Porro et al., 2019). An overlay of the S4 domain from the apo-like and the holo-like conformation, in which the two S4 domains are normalized to the linear outward facing part of the α-helix, predicts a similar picture: S4 is approximately linear in the apo form and reveals a kink with S272 as a hinge in the holo-conformation. While both negative voltage and ligand binding seem to favor kink formation in the S4 domain around a Serine hinge, they presumably achieve this in different manners. The force vectors on the S4 domain, which are elicited by release of cAMP from its biding site, are stronger on the upper part of the S4 helix, favoring a bending of this part toward the pore axis (Fig. 6 C). Negative voltage apparently

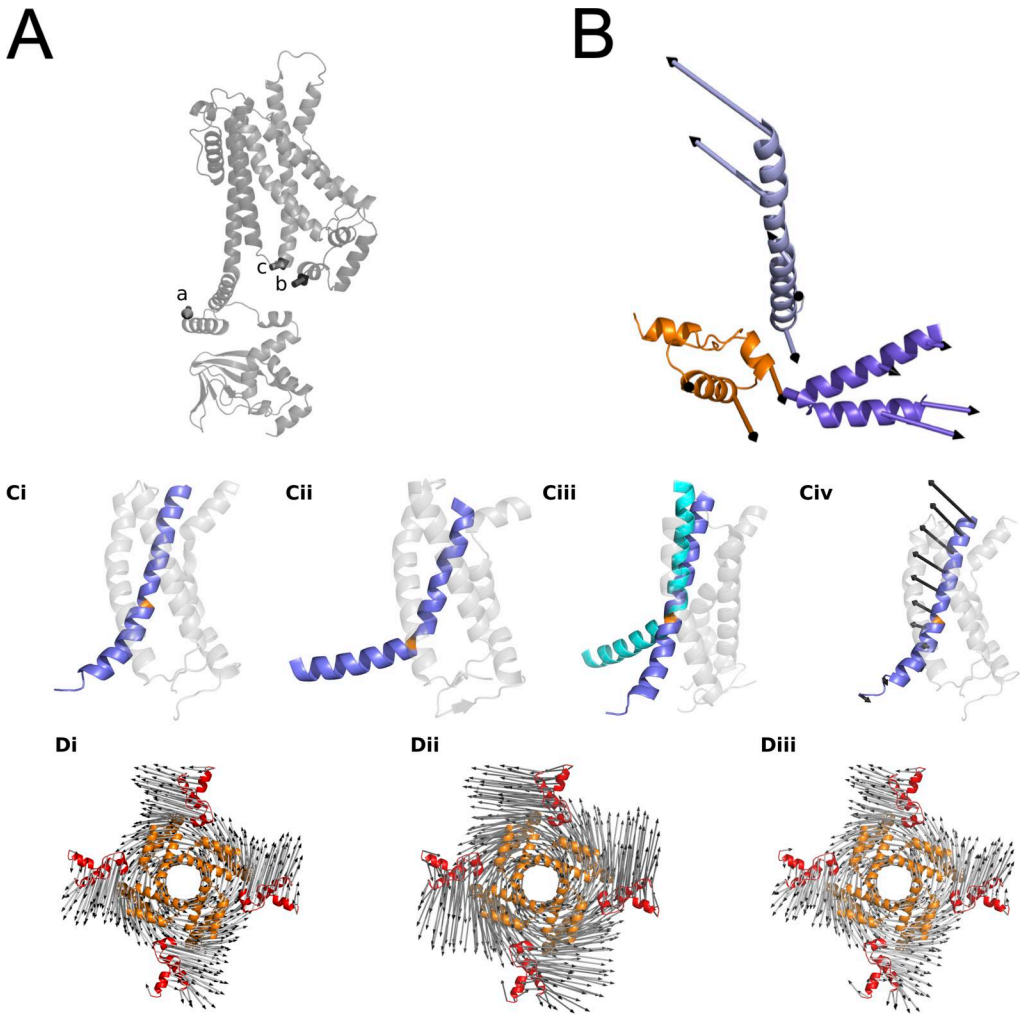

Figure 6. **LRT analysis to examine mechanical coupling between C-linker, HCND, and S4 helix in HCN1. (A)** Three positions in a HCN1 subunit in which forces in directions of arrows were applied to A425 in C-Linker (arrow a), R112 in b-helix of HCND (arrow b), and M287 on S4 (arrow c). **(B)** Three-dimensional organization and concerted movement of C-linker (purple), HCND (orange), and S4 (blue). The counterclockwise rotational movement of the C-linker (purple arrows) upon cAMP binding (arrow a in A) causes horizontal translocation of the HCND along tangent of C-linker displacement. Direct and indirect coupling of the HCND to TMDs evokes tilting of S4. The selected arrows show the direction of movements of all three domains after perturbing the elbow (arrow a in A). **(C)** Kink formation in S4 domain of HCN1 in response to negative voltage and ligand binding. **(C i–iv)** S4 domain (in blue) from cryo-EM HCN1 structures in depolarized (PDB 5U6O) (Ci) and hyperpolarized (PDB 6UQF (C ii) condition with kink formation around S272 (orange) (Lee and MacKinnon, 2017; Lee and MacKinnon, 2019). **(C iii)** S4 domain from same perspective as in C i/C ii with overlay of S4 conformation in apo-like (blue) and holo-like state (cyan). Structures predicted from LRT analysis of HCN1 following application of force to A425 in the C-linker (arrow a in A), which mimics cAMP binding (PDB 5U6O) (Groß et al., 2018; Porro et al., 2019). For comparison of LRT data in C iii with structures in C i/C ii, the S4 structures were normalized to the amino acids 270–272 in the hinge (in orange). **(C iv)** Apo-like structure from C iii with displacement vectors evoked by force application to A425 (arrow a in A). **(D)** LRT analysis to examine reciprocity of mechanical coupling between C-linker, HCND, and S4 helix in HCN1. HCN1 was perturbed in three different domains (arrows a–c in A) to elicit movement of C-linker and HCND. Images D i–D iii show C-linkers (in orange) and HCNDs (in red) as tetramers from extracellular perspective in response different perturbations. Irrespectively on whether the force was applied at the elbow by arrow a (D i), at the HCND by arrow b (D ii), or on the S4 domain by arrow c (D iii), the C-linker and the HCND exhibit the same rotational movement as apparent from the direction of the displacement vectors. See caption Fig. 5 for the magnitude/lengths of the arrows.

promotes more a bending of the lower part of the helix away from the pore.

Fig. 6 C iv depicts only the predicted tilting/bending movement of S4. Within the global protein, the LRT analysis predicts that this tilting motion also evokes, just like in the experimental structures of HCN1 (Lee and MacKinnon, 2019; Burtscher et al., 2024) and HCN4 (Saponaro et al., 2021), a directional displacement of helices S4, S5, and S6 with a concomitant outward movements of the C-terminal half of S4 and S5 (Groß et al., 2018). Moreover, the LRT prediction implies that this S4–S5 movement is linked to a rotation of S6 and, consequently, a widening of the pore entrance (Groß et al., 2018). The same S6 rotation/pore widening was later experimentally shown both in HCN1 (Burtscher et al., 2024) and in HCN4 (Saponaro et al., 2021) as a part of pore opening.

The finding that negative voltage and cAMP binding seem to favor a tilting movement of the S4 domain (Fig. 6 C) bears a potential explanation for the mechanisms by which ligand

binding reduces the energy barrier for voltage-dependent opening of HCN channels. The data suggest that the energy for imposing this crucial conformational change for channel opening may be lower when voltage and ligand binding work in a concerted manner on imposing this tilting of S4 than in the case of voltage alone. This interpretation is consistent with the experimental data according to which cAMP binding cannot open the channel but favors voltage-dependent channel activation (James and Zagotta, 2018).

The beauty of coarse-grained approaches with their low requirement for computational resources is that they allow an easy testing of model predictions. The above-mentioned data imply that C-linker, HCND, and VSD form a mechanical continuum, and that conformational changes in the C-linker can be transmitted in this manner via the HCND to the VSD. If this is true, the same flow of information should also occur in the opposite direction, e.g., from the VSD to the C-linker and presumably to the CNBD. A test of this prediction confirmed this assumption in that the critical rotational movement in the protein is elicited irrespectively on whether force is applied to the C-linker, the HCND, or the S4 helix (Fig. 6 D i–iii). Collectively, these data confirm the central position of the HCND as a mechanical connection, which couples in a bevel gear manner the CNBD with the VSD. A recent computational study that examined by elastic network analysis the mechanical connectivity between HCND and VSD in channels suggests that the flexibility of this connection changed during evolution. A high degree of flexibility is apparently crucial for an allosteric modulation of voltage gating by cAMP with the effect that the HCN isoforms 1, 2, and 4 are sensitive to this second messenger, while HCN3 and spHCN are not (Alvarez-Villagómez and Balleza, 2025, *Preprint*).

This view of HCN channels as a distinct mechanical continuum in which individual domains can communicate via long-range interactions connections also has implications for the development of drugs. By exploiting the knowledge of long-range interactions in these proteins, it should even be possible to modulate the impact of cAMP binding by small molecules, which bind on the extracellular side to HCN channel in sites that are mechanical affected by ligand binding.

Cooperativity of cAMP gating in HCN channels

The structures of tetrameric HCN channels exhibit an apparent fourfold symmetry in the TMPC as well as in their cytosolic CNBDs (Lee and MacKinnon, 2017; Saponaro et al., 2021). Despite this structural symmetry, functional data suggest an explicit asymmetric behavior in both cAMP binding and channel gating. For example, gating of HCN2 concatemers, which carry between 0 and 4 mutations in the cAMP-binding site, is best explained by a cooperativity between the ligand-binding sites (Liu et al., 1998; Ulens and Siegelbaum, 2003). The data advocate a scenario in which cAMP binding favors the formation of CNBD dimers and that ligand-mediated full channel opening is only occurring after a pairing of these dimers. More evidence for cooperativity in cAMP binding in HCN channel gating was derived from patch-clamp fluorometric recordings, a technique that monitors binding of a fluorescent cAMP analog to their binding site while simultaneously recording channel activation (Kusch et al., 2012). These data suggest that cAMP binds HCN2 with different modes of cooperativity depending on whether the channel is in a voltage-dependent closed or open state (Kusch et al., 2012; Thon et al., 2015). The most complex and physiological relevant mode of allostery occurs in the voltage-activated channel in which binding of a cAMP molecule to one binding site modulates the affinity of the remaining empty sites. Experimental data for this voltage-activated channel advocate a complex allosteric model for sequential binding with a positive-negative-positive cooperativity. It predicts that the affinity for binding of a second and fourth cAMP ligand is enhanced by a preceding binding step while binding of the third ligand molecule is penalized (Kusch et al., 2012).

The general importance of cooperativity in ligand binding to HCN channels in their closed state was later questioned by single-molecule studies in which the binding dynamics of cAMP to individual detergent-solubilized HCN1 and HNC2 channels was directly monitored at single protein level (White et al., 2021). In this study, the ligand molecules were found to bind independently to all four subunits, thus questioning a molecular basis for cooperative cAMP-mediated HCN channel gating. In contrast to that, subsequent measurements also with single-molecule resolution on HCN channels either in lipid nanodiscs (Idikuda et al., 2024, *Preprint*) or in isolated membrane patches (Kuschke et al., 2024) reported in contrast a distinct positive cooperativity. The affinity of each empty binding site occurred to increase as a function of a preceding binding step. Taken together, these data underpin that HCN channel proteins have an inherent tendency for a cooperative ligand binding; this allostery seems to be affected by membrane voltage and by constrains of the lipid bilayer on the channel protein (Idikuda et al., 2024, *Preprint*).

To further examine the question of cooperativity in cAMP-mediated gating of HCN channels with an independent computational approach, the ENM analysis of HCN in combination with LRT described before was employed (Kunzmann et al., 2024). The special twist of this study was that the force on the cAMP-binding site, which mimics the conformational change in cAMP binding, was not applied to all four subunits but only to individual binding sites in the tetramer (Fig. 7 A). It was reasoned that a local impact of one subunit should have no consequences on the remaining subunits in the case that ligand binding is noncooperative. If, however, the protein exhibits cooperativity between the ligand-binding sites, one should detect an impact of one subunit on the others.

The systematic analysis of the LRT data on the cryo-EM structures of HCN4 and HCN1 strongly supports a cooperativity in cAMP binding in these channels (Kunzmann et al., 2024). Stepwise binding generated in these channels, which were not in the voltage-activated state, essentially the same sequence of positive, negative, and positive cooperativity in the channel, which was observed in patch-clamp fluorometric recordings of the voltage-activated HCN2 channel (Fig. 7, B and C). The computational data further imply a scenario in which the initial cAMP-binding step increases the affinity for binding in the subunit diagonally opposite to the first binding monomer while

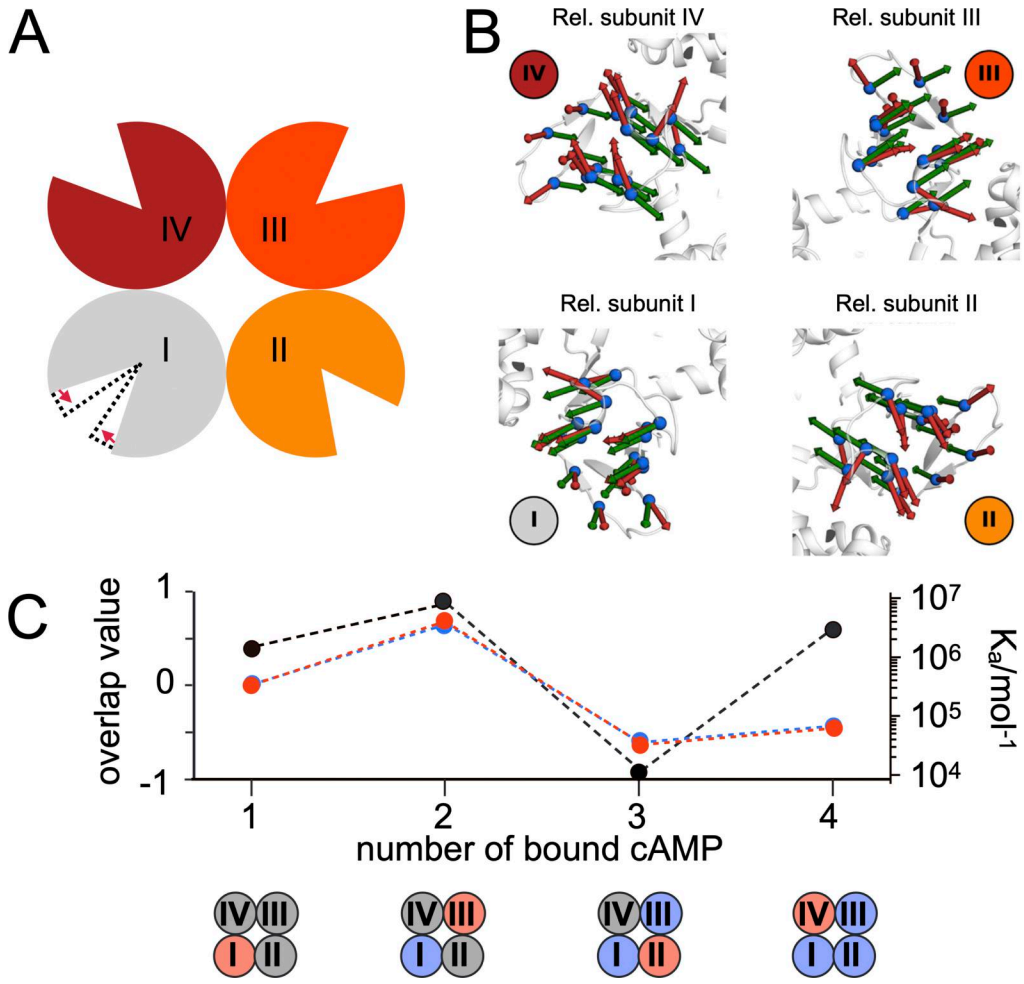

Figure 7. **Analysis of cooperativity in ligand binding to HCN channels by LRT. (A)** Principle of approach. Sketch of four CNBDS (I–IV) of HCN channel in apo state with empty cAMP-binding site (triangle). Forces (red arrows) applied to binding site in one subunit (I) mimic the binding site structure in cAMP-bound conformation (dotted line). **(B)** The forces for shifting ligand-binding site into holo-conformation (red arrows) are compared with the experimental structure displacements (green arrows) between apo- and holo-state of the binding sites from cryo-EM structures. Note that red and green arrows point in large in the same direction in subunit I and III (high positive overlap value) but into opposite directions in subunit II and IV (high negative overlap value). Hence, forces in monomer I reproduce its cAMP-bound state. The imposed holo-state in I also promotes conformational transition toward a cAMP-bound conformation in the opposite monomer III. This can be interpreted as positive cooperativity. Imposed binding in I in contrast disfavors ligand binding in lateral monomers II and IV, suggesting a negative cooperativity. **(C)** LRT-modeled sequential binding patterns of HCN1 (blue) and HCN4 (red) channels show in their overlap values the same pattern of positive and negative cooperativity as the experimentally derived K_a values for cAMP binding in HCN2 (black) by Kusch et al. (2012). Bottom row depicts in red the acutely perturbed subunit in the LRT analysis, proceeding perturbed subunits in blue, and unperturbed subunits in gray. Data in B and C reproduced with permission by Kunzmann et al. (2024). See caption Fig. 5 for the magnitude/lengths of the arrows.

imposing a negative effect on the adjacent monomers (Fig. 7 B). Unlike expected from the experimental data (Idikuda et al., 2024, *Preprint*), this distinct pattern of cooperativity seemed to be unaffected by the presence or absence of a membrane around a protein (Kunzmann et al., 2024). Such a potential constraining impact of a membrane round a protein can be considered in the vibrational analysis of the protein by an explicit ANM for a bilayer (Lezon and Bahar, 2012; Lomize et al., 2022; Kunzmann et al., 2024).

To answer the question if this kind of cooperative behavior is a specific feature of HCN channels, the same analysis was performed with structurally related channels with active or inactive cAMP-binding sites. The results showed that also the cyclic nucleotide gated (CNG) channel TAX4 and the Kv channel KAT1 exhibit a similar but much less pronounced pattern of cooperativity between the ligand-binding sites. Interesting to mention in this context is that an independent anisotropic network analysis of the human CNG channel (CNGA3) (Gofman et al., 2014) found the same positive and negative interplay between CNBDs as in the analysis with LRT (Kunzmann et al., 2024). Both studies propose that the pairs of diagonal CNBDs move in an alternating manner toward and away from each other.

Taken together, the data suggest that cooperativity between subunits is an inherent property of channel proteins with the same overall architecture. In the case of HCN channels, this cooperative interaction between ligand-binding sites was presumably optimizing during evolution to allow the fine tuning of cAMP-mediated gating in these channels. Inherent structural

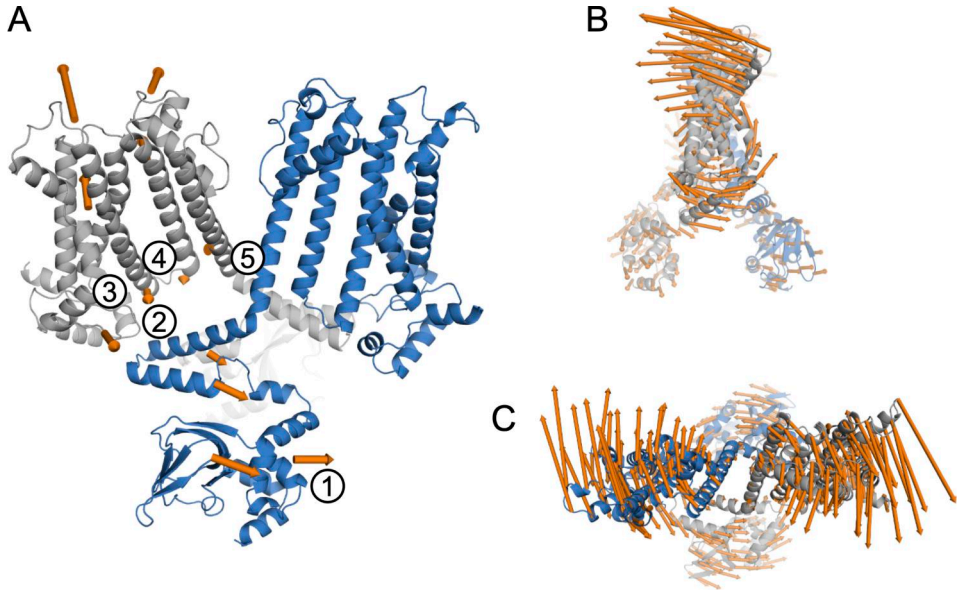

Figure 8. **Implications of ENM/LRT analysis for cAMP-mediated gating of HCN channels. (A–C)** Side view of two opposite subunits of HCN channel as in Fig 1. Selected arrows indicate main directions of conformational movements of critical domains throughout the protein following cAMP binding. The numbers suggest functional consequences of these movements for cAMP-mediated gating: (1) ligand binding in one monomer has positive and negative impacts on cooperative binding to remaining monomers; (2) the C-linker approaches S4; (3) rotational movement of the C-linker causes via HCND a tilting of the S4 domain; (4) tilting of S4 promotes opening of a gating canal for modulation of electrical field surrounding S4. (5) Opening of the inner gate is promoted. Side view (B) and top view (C) of image in A showing how cAMP binding promotes a right handed (A and B) or anticlockwise (C) rotation in the cytosolic domain (opaque) and how this is translated by the C-linker into a tilting movement of the transmembrane domains (full color) in the opposite direction. See caption Fig. 5 for the magnitude/lengths of the arrows.

constrains in the HCN channel tetramer presumably favor a collective alternating movement of diagonal CNBDs toward and away from each other in the voltage-activated state of the channel. In the next step, it would be interesting to examine how the voltage sensor domain in the active and inactive state affects the geometry and topology of the CNBD.

Conclusions

This review underscores that coarse grained computational methods are, in combination with high-resolution structures of these proteins, able to distill relevant mechanical connections and conformational movements in the complex HCN channels. The combination of ENMs with LRT has predicted a number of conformational movements in these channels in the context of cAMP binding that were either confirmed later by experimental structures or supported by functional data from HCN channels. This underlines that the respective methods are, in spite of their simplicity, suitable for understanding macroscopic, long-range interactions in these channels like the modulation of voltage gating by ligand binding. The good agreement between experimental structural and functional data on one side and model predictions from coarse grained simulations on the other side provide some important information: because ENM/LRT simulations are not considering any detailed chemical interactions in proteins, the geometry and topology of HCN channels must be such that small local fluctuations and large collective movements of different domains are an inherent "material" property in these proteins; under equilibrium conditions, the degree of freedom of movements is to some extent limited and determined by their global architecture. Critical interactions between amino acids in these proteins like salt bridges, hydrogen bonds, or hydrophobic interactions, which were found important in cAMP-mediated gating of HCN channels (e.g., Porro et al., 2019; Porro et al., 2020; Porro et al., 2024; Kondapuram et al., 2022) must be understood as interactions, which enforce and physically stabilize conformational movements, which are already inherent in these proteins.

The systematic analysis of conformational changes in HCN channels following binding of cAMP to its binding site in the CNBD is summarized in Fig. 8, A and B. Ligand binding promotes a sideward movement of the CNBD (arrows a). This generates an iris-like, anticlockwise rotation of the C-linker (arrows b). The rotational movement of the C-linker pulls the HCND and the lower part of the S4 domain along the tangential axis of the rotation (arrow c). The consequence is a tilting of the transmembrane domains, including the S4 domain (arrows d) relative to the z-axis of the lipid bilayer. All these movements are reversed by a loss of cAMP from its binding site.

The conformational changes in HCN channels detected by the combined ENM/LRT analysis have some implications for cAMP-mediated gating, which are summarized in Fig. 8 A: (1) ligand binding in one monomer has positive and negative impacts on binding domains in the remaining monomers, which can explain the complex pattern of cAMP-mediated cooperativity in HCN gating. (2) The C-linker approaches S4, and (3) the rotational movement of the C-linker favors, via the HCND, a tilting of the S4 domain. (4) Tilting of S4 away from S5 promotes opening of a

"gating canal," an aqueous structure which is postulated to modulate the electrical properties of the electrical field surrounding S4. (5) The conformational transitions in the protein promote opening of the inner gate. Important to mention at this point is that cAMP binding is by itself not able to open HCN channels; it only decreases the energy barrier for an opening of the channels by negative voltage. Hence, within the limitations of the coarse-grained method, which is not observing actual movements in the protein, we must interpret these data in a sense that cAMP binding lowers the energy for the real physical movement of the S4 domain and the opening of the inner gate by negative voltage.

Acknowledgments

Crina M. Nimigean served as editor.

We thank Dr. S. Weißgraeber (TU Darmstadt) for generating the video in Fig. 4. The authors are grateful to anonymous reviewers who provided valuable insight and thereby improved the manuscript.

This work was funded by Deutsche Forschungsgemeinschaft (grants HA5261/6-1 to K. Hamacher and TH558/34-1 to G. Thiel), a Foundation Leducq Research Grant (TNF FANTASY- 19CVD03 to A. Moroni and D. DiFrancesco) and by the Ministero Della Ricerca (MUR) Progetti di Rilevante Interesse Nationale (PRIN) (2022EMA8FA to A. Moroni).

Author contributions: Magnus Behringer: visualization and writing—original draft, review, and editing. Jan Krumbach: visualization and writing—original draft. Alessandro Porro: visualization and writing—original draft. Andrea Saponaro: writing—review and editing. Dario DiFrancesco: writing—review and editing. Anna Moroni: funding acquisition and writing—review and editing. Kay Hamacher: conceptualization, formal analysis, funding acquisition, methodology, project administration, software, supervision, and writing—original draft, review, and editing. Gerhard Thiel: conceptualization and writing—original draft, review, and editing.

Disclosures: The authors declare no competing interests exist.

Submitted: 23 September 2025
Revised: 10 February 2026
Accepted: 5 March 2026

References

Akimoto, M., Z. Zhang, S. Boulton, R. Selvaratnam, B. VanSchouwen, M. Gloyd, E.A. Accili, O.F. Lange, and G. Melacini. 2014. A mechanism for the auto-inhibition of hyperpolarization-activated cyclic nucleotide-gated (HCN) channel opening and its relief by cAMP. *J. Biol. Chem.* 289:22205–22220. https://doi.org/10.1074/jbc.M114.572164

Alvarez-Villagómez, K.G., and D. Balleza. 2025. Structural determinants of voltage sensitivity in hyperpolarization-activated ion channels and their persistence in the evolutionary scale. Res. Square. https://doi.org/10.21203/rs.3.rs-8117147/v1 (Preprint posted November 26, 2025).

Atilgan, A.R., S.R. Durell, R.L. Jernigan, M.C. Demirel, O. Keskin, and I. Bahar. 2001. Anisotropy of fluctuation dynamics of proteins with an elastic network model. *Biophys. J.* 80:505–515. https://doi.org/10.1016/S0006-3495(01)76033-X

Bahar, I., R.T. Lezon, L.W. Yang, and E. Eyal. 2010. Global dynamics of proteins: Bridging between structure and function. *Annu. Rev. Biophys.* 39: 23–42. https://doi.org/10.1146/annurev.biophys.093008.131258

Bauer, D., J. Wissmann, A. Moroni, G. Thiel, and K. Hamacher. 2022. Weak cation selectivity in HCN channels results from K^+-mediated release of Na^+ from the selectivity filter. *Function*. 3:zqac019. https://doi.org/10.1093/function/zqac019

Bell, D.C., H. Yao, R.C. Saenger, J.H. Riley, and S.A. Siegelbaum. 2004. Changes in local S4 environment provide a voltage-sensing mechanism for mammalian hyperpolarization–activated HCN channels. *J. Gen. Physiol.* 123:5–19. https://doi.org/10.1085/jgp.200308918

Benndorf, K., U. Enke, D. Tewari, J. Kusch, H. Liu, H. Sun, R. Schmauder, and C. Sattler. 2025. Subunit-specific conductance of single homomeric and heteromeric HCN pacemaker channels at femtosiemens resolution. *Proc. Natl. Acad. Sci. USA*. 122:e2422533122. https://doi.org/10.1073/pnas.2422533122

Bucchi, A., M. Baruscotti, and D. DiFrancesco. 2002. Current-dependent block of rabbit sino-atrial node I(f) channels by ivabradine. *J. Gen. Physiol.* 120: 1–13. https://doi.org/10.1085/jgp.20028593

Burtscher, V., J. Mount, J. Huang, J. Cowgill, Y. Chang, K. Bickel, J. Chen, P. Yuan, and B. Chanda. 2024. Structural basis for hyperpolarization-dependent opening of human HCN1 channel. *Nat. Commun.* 15:5216. https://doi.org/10.1038/s41467-024-49599-x

Chennubhotla, C., and I. Bahar. 2007. Markov methods for hierarchical coarse-graining of large protein dynamics. *J. Comp. Biol.* 14:765–776. https://doi.org/10.1089/cmb.2007.R015

Craven, K.B., and W.N. Zagotta. 2004. Salt bridges and gating in the COOH-terminal region of HCN2 and CNGA1 channels. *J. Gen. Physiol.* 124: 663–677. https://doi.org/10.1085/jgp.200409178

Craven, K.B., N.B. Olivier, and W.N. Zagotta. 2008. C-terminal movement during gating in cyclic nucleotide-modulated channels. *J. Biol. Chem.* 283:14728–14738. https://doi.org/10.1074/jbc.M710463200

Das, A., M. Gur, M.H. Cheng, S. Jo, I. Bahar, and B. Roux. 2014. Exploring the conformational transitions of biomolecular systems using a simple two-state anisotropic network model. *PLOS Comput. Biol.* 10:1–17. https://doi.org/10.1371/journal.pcbi.1003521

DiFrancesco, D. 1982. Block and activation of the pace-maker channel in calf Purkinje fibres: Effects of potassium, caesium and rubidium. *J. Physiol.* 329:485–507. https://doi.org/10.1113/jphysiol.1982.sp014315

DiFrancesco, D. 1986. Characterization of single pacemaker channels in cardiac sino-atrial node cells. *Nature*. 324:470–473. https://doi.org/10.1038/324470a0

DiFrancesco, D., and P. Tortora. 1991. Direct activation of cardiac pacemaker channels by intracellular cyclic AMP. *Nature*. 351:145–147. https://doi.org/10.1038/351145a0

Elbahnsi, A., J. Cowgill, V. Burtscher, L. Wedemann, L. Zeckey, B. Chanda, and L. Delemotte. 2023. Interplay between VSD, pore, and membrane lipids in electromechanical coupling in HCN channels. *Elife*. 12:e80303. https://doi.org/10.7554/eLife.80303

Eom, K., S.C. Baek, J.H. Ahn, and S. Na. 2007. Coarse-graining of protein structures for the normal mode studies. *J. Comput. Chem.* 28:1400–1410. https://doi.org/10.1002/jcc.20672

Flynn, G.E., and W.N. Zagotta. 2018. Insights into the molecular mechanism for hyperpolarization-dependent activation of HCN channels. *Proc. Natl. Acad. Sci. USA*. 115:E8086–E8095. https://doi.org/10.1073/pnas.1805596115

Goldschen-Ohm, M.P., V.A. Klenchin, D.S. White, J.B. Cowgill, Q. Cui, R.H. Goldsmith, and B. Chanda. 2016. Structure and dynamics underlying elementary ligand binding events in human pacemaking channels. *Elife*. 5:e20797. https://doi.org/10.7554/eLife.20797

Gofman, Y., C. Schärfe, D.S. Marks, T. Haliloglu, and N. Ben-Tal. 2014. Structure, dynamics and implied gating mechanism of a human cyclic nucleotide-gated channel. *PLoS Comput. Biol.* 10:e1003976. https://doi.org/10.1371/journal.pcbi.1003976

Groß, C., K. Hamacher, K. Schmitz, and S. Jager. 2017. Cleavage product accumulation decreases the activity of cutinase during PET hydrolysis. *J. Chem. Inf. Model.* 57:243–255. https://doi.org/10.1021/acs.jcim.6b00556

Groß, C., A. Saponaro, B. Santoro, A. Moroni, G. Thiel, and K. Hamacher. 2018. Mechanical transduction of cytoplasmic-to-transmembrane-domain movements in a hyperpolarization-activated cyclic nucleotide–gated cation channel. *J. Biol. Chem.* 293:12908–12918. https://doi.org/10.1074/jbc.RA118.002139

Haliloglu, T., I. Bahar, and B. Erman. 1997. Gaussian dynamics of folded proteins. *Phys. Rev. Lett.* 79:3090–3093. https://doi.org/10.1103/physrevlett.79.3090

Hamacher, K. 2011. Free energy of contact formation in proteins: Efficient computation in the elastic network approximation. *Phys. Rev. E. Stat. Nonlin. Soft. Matter. Phys.* 84:016703. https://doi.org/10.1103/PhysRevE.84.016703

Hamacher, K., and J.A. McCammon. 2006. Computing the amino acid specificity of fluctuations in biomolecular systems. *J. Chem. Theo. Comp.* 2: 873–878. https://doi.org/10.1021/ct050247s

Hamacher, K., J. Trylska, and J.A. McCammon. 2006. Dependency map of proteins in the small ribosomal subunit. *PLoS Comput. Biol.* 2:e10–e2006. https://doi.org/10.1371/journal.pcbi.0020010

Hayward, S., and B.L. de Groot. 2008. Normal modes and essential dynamics. *In* Molecular Modeling of Proteins, Methods Molecular Biology™. A. Kukol, editor. Humana Press, Totowa, NJ. 89–106. https://doi.org/10.1007/978-1-59745-177-2_5

Hoffgaard, F., S.M. Kast, A. Moroni, G. Thiel, and K. Hamacher. 2015. Tectonics of a K^+ channel: The importance of the N-terminus for channel gating. *Biochim. Biophys. Acta.* 1848:3197–3204. https://doi.org/10.1016/j.bbamem.2015.09.015

Idikuda, V., S.R. Chowdhury, Y. Chang, Q. Ren, H. Bao, R.H. Goldsmith, and B. Chanda. 2024. Lipid bilayers determine the allostery but not intrinsic affinity of cAMP binding to pacemaker channels. *bioRxiv*. https://doi.org/10.1101/2024.12.23.630133 (Preprint posted December 24, 2024).

Ikeguchi, M., J. Ueno, M. Sato, and A. Kidera. 2005. Protein structural change upon ligand binding: Linear response theory. *Phys. Rev. Lett.* 94:078102. https://doi.org/10.1103/PhysRevLett.94.078102

James, Z.M., and W.N. Zagotta. 2018. Structural insights into the mechanisms of CNBD channel function. *J. Gen. Physiol.* 150:225–244. https://doi.org/10.1085/jgp.201711898

Kasimova, M.A., D. Tewari, J.B. Cowgill, W.C. Ursuleaz, J.L. Lin, L. Delemotte, and B. Chanda. 2019. Helix breaking transition in the S4 of HCN channel is critical for hyperpolarization-dependent gating. *Elife*. 8: e53400. https://doi.org/10.7554/eLife.53400

Kondrashov, D.A. 2011. Using normal mode analysis in teaching mathematical modeling to biology students. *Math. Model. Nat. Phenom.* 6:278–294. https://doi.org/10.1051/mmnp/20116615

Kim, E.D., X. Wu, S. Lee, G.R. Tibbs, K.P. Cunningham, E. Di Zanni, M.E. Perez, P.-A. Goldstein, A. Accardi, H.P. Larsson, and C.M. Nimigean. 2024. Propofol rescues voltage-dependent gating of HCN1 channel epilepsy mutants. *Nature*. 632:451–459. https://doi.org/10.1038/s41586-024-07743-z

Kondapuram, M., B. Frieg, S. Yüksel, T. Schwabe, C. Sattler, M. Lelle, A. Schweinitz, R. Schmauder, K. Benndorf, H. Gohlke, and J. Kusch. 2022. Functional and structural characterization of interactions between opposite subunits in HCN pacemaker channels. *Commun. Biol.* 5:430. https://doi.org/10.1038/s42003-022-03360-6

Kunzmann, P., A. Krumbach, A. Saponaro, G. Moroni, and K. Hamacher. 2024. Anisotropic network analysis of open/closed HCN4 channel advocates asymmetric subunit cooperativity in cAMP modulation of gating. *J. Chem. Info. Mod.* 64:4727–4738. https://doi.org/10.1021/acs.jcim.4c00360

Kusch, J., S. Thon, E. Schulz, C. Biskup, V. Nache, T. Zimmer, S. Seifert, F. Schwede, and K. Benndorf. 2012. How subunits cooperate in cAMP-induced activation of homotetrameric HCN2 channels. *Nat. Chem. Biol.* 8:162–169. https://doi.org/10.1038/nchembio.747

Kuschke, S., S. Thon, T. Schwabe, K. Benndorf, and R. Schmauder. 2024. cAMP binding to closed pacemaker ion channels is cooperative. *Proc. Natl. Acad. Sci. USA*. 121:e2315132121. https://doi.org/10.1073/pnas.2315132121

Krumbach, J.H., D. Bauer, A.S. Sharifzadeh, A. Saponaro, R. Lautenschläger, K. Lange, O. Rauh, D. DiFrancesco, A. Moroni, G. Thiel, and K. Hamacher. 2023. Probing HCN4 filter dynamics and selectivity with a series of alkali metal cations. *J. Gen. Physiol.* 155:e202313364. https://doi.org/10.1085/jgp.202313364

Lee, C.H., and R. MacKinnon. 2017. Structures of the human HCN1 hyperpolarization-activated channel. *Cell*. 168:111–120.e11. https://doi.org/10.1016/j.cell.2016.12.023

Lee, C.H., and R. MacKinnon. 2019. Voltage sensor movements during hyperpolarization in the HCN channel. *Cell*. 179:1582–1589.e7. https://doi.org/10.1016/j.cell.2019.11.006

Lee, B., K.I. White, M. Socolich, M.A. Klureza, R. Henning, V. Srajer, R. Ranganathan, and D.R. Hekstra. 2025. Direct visualization of electric-field-stimulated ion conduction in a potassium channel. *Cell*. 188: 77–88.e15. https://doi.org/10.1016/j.cell.2024.12.006

Lezon, T.R., and I. Bahar. 2012. Constraints imposed by the membrane selectively guide the alternating access dynamics of the glutamate transporter GltPh. *Biophys. J.* 102:1331–1340. https://doi.org/10.1016/j.bpj.2012.02.028

Lolicato, M., M. Nardini, S. Gazzarrini, S. Möller, D. Bertinetti, F.W. Herberg, M. Bolognesi, H. Martin, M. Fasolini, J.A. Bertrand, et al. 2011. Insights into the differential response to cAMP of the pacemaker channel isoform HCN1. *J. Biol. Chem.* 286:44811–44820. https://doi.org/10.1074/jbc.M111.297606

Lezon, T.R., I.H. Shrivastava, Z. Yang, and I. Bahar. 2009. Elastic Network Models for Biomolecular Dynamics: Theory and Application to Membrane Proteins and Viruses. *In* World Scientific Lecture Notes in Complex Systems. World Scientific, Singapore. pp. 129–158.

Lomize, A.L., S.C. Todd, and I.D. Pogozheva. 2022. Spatial arrangement of proteins in planar and curved membranes by PPM 3.0. *Protein Sci.* 31: 209–220. https://doi.org/10.1002/pro.4219

Liu, D.T., D.R. Tibbs, P. Paoletti, and S.A. Siegelbaum. 1998. Constraining ligand-binding site stoichiometry suggests that a cyclic nucleotide-gated channel is composed of two functional dimers. *Neuron*. 21: 235–248. https://doi.org/10.1016/s0896-6273(00)80530-9

Lyashchenko, A.K., and G.R. Tibbs. 2008. Ion binding in the open HCN pacemaker channel pore: Fast mechanisms to shape "slow" channels. *J. Gen. Physiol.* 131:227–243. https://doi.org/10.1085/jgp.200709868

Mahajan, S., and Y.H. Sanejouand. 2015. On the relationship between low-frequency normal modes and the large-scale conformational changes of proteins. *Arch. Biochem. Biophys.* 567:59–65. https://doi.org/10.1016/j.abb.2014.12.020

Marchesi, A., X. Gao, R. Adaixo, J. Rheinberger, H. Stahlberg, C. Nimigean, and S. Scheuring. 2018. An iris diaphragm mechanism to gate a cyclic nucleotide-gated ion channel. *Nat. Commun.* 9:3978. https://doi.org/10.1038/s41467-018-06414-8

Miyashita, O., J.N. Onuchic, and P.G. Wolynes. 2003. Nonlinear elasticity, proteinquakes, and the energy landscapes of functional transitions in proteins. *Proc. Nat. Acad. Sci. USA*. 100:12570–12575. https://doi.org/10.1073/pnas.2135471100

Morgan, R.T., S. Motta, E. Gil-Iturbe, B. Bhattacharjee, M.T. Anwar, G. Di Muccio, A. Romagnoli, B. Mishra, K.U. Ashraf, I. Bang, et al. 2025. Mechanistic snapshots of lipid-linked sugar transfer. *Nat. Commun.* 16: 11044. https://doi.org/10.1038/s41467-025-66769-7

Moroni, A., A. Barbuti, C. Altomare, C. Viscomi, J. Morgan, M. Baruscotti, and D. DiFrancesco. 2000. Kinetic and ionic properties of the human HCN2 pacemaker channel. *Pflugers Arch.* 439:618–626. https://doi.org/10.1007/s004249900225

Penrose, R. 1955. A generalized inverse for matrices. *Math. Pro. Cambridge Philol. Soc.* 51:406–413. https://doi.org/10.1017/S0305004100030401

Press, W.H., S.A. Teufolsky, W.T. Vetterling, and B.P. Flannery. 2007. Numerical Recipes 3rd Edition: The Art of Scientific Computing. Third edition. Cambride University Press, Cambridge.

Porro, A., A. Saponaro, F. Gasparri, D. Bauer, C. Groß, M. Pisoni, G. Abbandonato, K. Hamacher, B. Santoro, G. Thiel, and A. Moroni. 2019. The HCN domain couples voltage gating and cAMP response in hyperpolarization-activated cyclic nucleotide-gated channels. *Elife*. 8. e49672. https://doi.org/10.7554/eLife.49672

Porro, A., G. Thiel, A. Moroni, and A. Saponaro. 2020. Cyclic AMP regulation and its command in the pacemaker channel HCN4. *Front. Physiol.* 11:771. https://doi.org/10.3389/fphys.2020.00771

Porro, A., A. Saponaro, R. Castelli, B. Introini, A.H. Alkotob, G. Ranjbari, U. Enke, J. Kusch, K. Benndorf, B. Santoro, et al. 2024. A high affinity switch for cAMP in the HCN pacemaker channels. *Nat. Commun.* 15:843. https://doi.org/10.1038/s41467-024-45136-y

Puljung, M.C., H.A. DeBerg, W.N. Zagotta, and S. Stoll. 2014. Double electron-electron resonance reveals cAMP-induced conformational change in HCN channels. *Proc. Natl. Acad. Sci. USA*. 111:9816–9821. https://doi.org/10.1073/pnas.1405371111

Robinson, R.B., and S.A. Siegelbaum. 2003. Hyperpolarization-activated cation currents: From molecules to physiological function. *Annu. Rev. Physiol.* 65: 453–480. https://doi.org/10.1146/annurev.physiol.65.092101.142734

Rothberg, B.S., K.S. Shin, and G. Yellen. 2003. Movements near the gate of a hyperpolarization-activated cation channel. *J. Gen. Physiol.* 122:501–510. https://doi.org/10.1085/jgp.200308928

Sanejouand, Y.-H. 2013. Elastic network models: Theoretical and empirical foundations. *In* Biomolecular Simulations: Methods and Protocols, Methods in Molecular Biology. L. Monticelli, and E. Salonen, editors. Humana Press, Totowa, NJ. 601–616. https://doi.org/10.1007/978-1-62703-017-5_23

Saponaro, A., S.R. Pauleta, F., Cantini, M. Matzapetakis, C. Hammann, C. Donadoni, L. Hu, G. Thiel, L. Banci, B. Santoro, and A. Moroni. 2014. Structural basis for the mutual antagonism of cAMP and TRIP8b in

regulating HCN channel function. *Proc. Natl. Acad. Sci. USA*. 111: 14577–14582. https://doi.org/10.1073/pnas.1410389111

Saponaro, A., D. Bauer, H. Giese, P. Swuec, A. Porro, F. Gasparri, A.S. Sharifzadeh, A. Chaves-Sanjuan, L. Alberio, G. Parisi, et al. 2021. Gating movements and ion permeation in HCN4 pacemaker channels. *Mol. Cells*. 81:1–15. https://doi.org/10.1016/j.molcel.2021.05.033

Saponaro, A., J.H. Krumbach, A. Chaves-Sanjuan, A.S. Sharifzadeh, A. Porro, R. Castelli, K. Hamacher, M. Bolognesi, D. DiFrancesco, O.B. Clarke, et al. 2024. Structural determinants of Ivabradine block of the open pore of HCN4. *Proc. Natl. Acad. Sci. USA*. 121:e2402259121. https://doi.org/10.1073/pnas.2402259121

Saponaro, A., and D. DiFrancesco. 2025. Structure mirroring function: What's the 'matter' with the funny current? *J Physiol*. https://doi.org/10.1113/JP287209

Shrivastava, I.H., and I. Bahar. 2006. Common mechanism of pore opening shared by five different potassium channels. *Biophys. J.* 90:3929–3940. https://doi.org/10.1529/biophysj.105.080093

Thon, S., E. Schulz, J. Kusch, and K. Benndorf. 2015. Conformational flip of nonactivated HCN2 channel subunits evoked by cyclic nucleotides. *Biophys. J.* 109:2268–2276. https://doi.org/10.1016/j.bpj.2015.08.054

Tirion, M.M. 1996. Large amplitude elastic motions in proteins from a single-parameter, atomic analysis. *Phys. Rev. Lett.* 77:1905–1908. https://doi.org/10.1103/PhysRevLett.77.1905

Ulens, C., and S.A. Siegelbaum. 2003. Regulation of hyperpolarization- activated HCN channels by cAMP through a gating switch in binding domain symmetry. *Neuron*. 40:959–970. https://doi.org/10.1016/s0896-6273(03)00753-0

Weißgraeber, S.A. Saponaro, G. Thiel, and K. Hamacher. 2017. A reduced mechanical model for cAMP modulated gating in HCN channels. *Sci. Rep.* 7:40168. https://doi.org/10.1038/srep40168

White, D.S., S. Chowdhury, V. Idikuda, R. Zhang, S.T. Retterer, R. Goldsmith, and B. Chanda. 2021. cAMP binding to closed pacemaker ion channels is non-cooperative. *Nature*. 595:606–610. https://doi.org/10.1038/s41586-021-03686-x

Wilson, E.B. 1941. Some mathematical methods for the study of molecular vibrations. *J. Chem. Phys.* 9:76–84. https://doi.org/10.1063/1.1750829

Xu, X., Z.V. Vysotskaya, Q. Liu, and L. Zhou. 2010. Structural basis for the cAMP-dependent gating in the human HCN4 channel. *J. Biol. Chem.* 285: 37082–37091. https://doi.org/10.1074/jbc.M110.152033

Yu, B., Q. Lu, J. Li, X. Cheng, H. Hu, Y. Li, T. Che, Y. Hua, H. Jiang, Y. Zhang, et al. 2024. Cryo-EM structure of human HCN3 channel and its regulation by cAMP. *J. Biol. Chem.* 300:107288. https://doi.org/10.1016/j.jbc.2024.107288

Zagotta, W., N. Olivier, K. Black, E.C. Young, R. Olson, and E. Gouaux. 2003. Structural basis for modulation and agonist specificity of HCN pacemaker channels. *Nature*. 425:200–205. https://doi.org/10.1038/nature01922

Zhao, Y., X. Zhang, L. Liu, F. Hu, F. Chang, Z. Han, and C. Li. 2024. Insights into activation dynamics and functional sites of inwardly rectifying potassium channel Kir3.2 by an elastic network model combined with perturbation methods. *J. Phys. Chem. B*. 128:1360–1370. https://doi.org/10.1021/acs.jpcb.3c06739

Supplemental material

Video 1. **Concerted movements in synthetic HCN channel after release of cAMP from ligand binding site.** The holo- to apo-transition causes a torsion like movement of the C-imker away from the membrane embedded part of the protein.